machines

MDPI

Communication

Investigation of the Temperature Effects on Copper Losses in Hairpin Windings

Mohammad Soltani *, Stefano Nuzzo, Davide Barater and Giovanni Franceschini

Department of Engineering Enzo Ferrari, University of Modena and Reggio Emilia, 41125 Modena, Italy
* Correspondence: mohammad.soltani@unimore.it

Abstract: Today, an extensive electrification is occurring in all industrial sectors, with a special interest seen in the automotive and aerospace industries. The electric motor, surely, is one of the main actors in this context, and an ever-increasing effort is spent with the aim of improving its efficiency and torque density. Hairpin windings are one of the recent technologies which are implemented onto the stator of the electric motor. Compared to conventional random windings, it inherently features lower DC resistance, higher fill factor, better thermal performance, improved reliability, and an automated manufacturing process. However, its bottleneck is the high ohmic losses at high-frequency operations due to skin and proximity effects (AC losses), resulting in a negative impact on the temperature map of the machine. Nevertheless, while it is well-known that DC losses increase linearly with the operating temperatures, the AC losses trend needs further insight. This paper demonstrates that operating the machine at higher temperatures could be beneficial for overall efficiency, especially at high-frequency operations. This suggests that a paradigm shift is required for the design of electric motors equipped with hair-pin windings, which should therefore focus on a temperature-oriented approach. In addition, the effect of the rotor topology on AC losses, which is often overlooked, is also considered in this paper. The combination of these effects is used to carry out observations and, eventually, to provide design recommendations. Finite element electromagnetic and thermal evaluations are performed to prove the findings of this research.

Keywords: hairpin winding; copper loss; propulsion motor; thermal analysis

Citation: Soltani, M.; Nuzzo, S.; Barater, D.; Franceschini, G. Investigation of the Temperature Effects on Copper Losses in Hairpin Windings. *Machines* **2022**, *10*, 715. https://doi.org/10.3390/machines10080715

Academic Editor: Ignacio González Prieto

Received: 1 June 2022
Accepted: 17 August 2022
Published: 20 August 2022

1. Introduction

Extensive research and development are currently taking place in the transportation field, where the electrification of vehicles plays one of the most critical roles in mitigating emissions and maximizing efficiency [1–3].

One of the key elements of the powertrain of hybrid electric vehicles (HEVs) and battery electric vehicles (BEVs) is the electrical machine. Nowadays, from the viewpoint of giving priority to the torque density of components, permanent magnet synchronous machines (PMSM) are widely implemented as propulsion motors in traction applications [4].

Of the techniques used to maximize the power density of electric machines, the design for high operating speeds is one of the most effective and straightforward. Nevertheless, this results in higher operating fundamental frequencies, which in turn means increased iron and ohmic losses, as well as more structural and reliability challenges [5].

When operating at a relatively low frequency, the current distribution in the armature conductors is usually uniform. In higher frequency ranges, skin and proximity effects can occur if no suitable precautions are taken, leading to higher conductors' resistances and losses [6]. Different winding methods have been introduced to mitigate these phenomena, such as Litz wires [7]. However, these feature a low copper-to-insulation ratio within the slot (fill factor), high manufacturing costs, and complex shaping and impregnation, making them suitable for very high-frequency applications only [8]. Transport applications, and in particular automotive ones, are rather cost-effective, and thus the most competitive

solution is the random winding, characterized by strands with a higher cross-section than those used in the Litz wire [9]. Although the random winding represents a good trade-off between costs and performance, its fill factor is low and, above the 1 kHz range, skin and proximity effects can still occur. In addition, the random distribution of conductors within the slots can make the winding voltage distribution uneven, thus impacting the overall reliability [5].

Hairpin windings are gaining popularity in traction applications [10]. This technology nearly doubles the fill factor compared to traditional random windings, further improving the overall performance metrics. Its main inherent advantages are lower DC resistance, higher fill factor, better thermal slot conductivity, improved voltage distribution, and an automated manufacturing process, which make hairpin windings suitable for the automotive field [11–14].

Considering all the above, combining PMSMs with hairpin windings maximizes the torque density of the motor itself and, consequently, of the powertrain and the vehicle. However, the biggest challenge of hairpin windings is the high losses at high-frequency operations (namely AC losses). In Figure 1, an example of the current density map in 6 hairpin legs within a motor slot is shown. As seen, in some of the conductors, the current density is not uniformly distributed, thus causing an increase in the equivalent resistance and losses. In the general example shown below, the frequency has been set at a relatively high value, i.e., 1 kHz, aiming to highlight the abovementioned high-frequency phenomena.

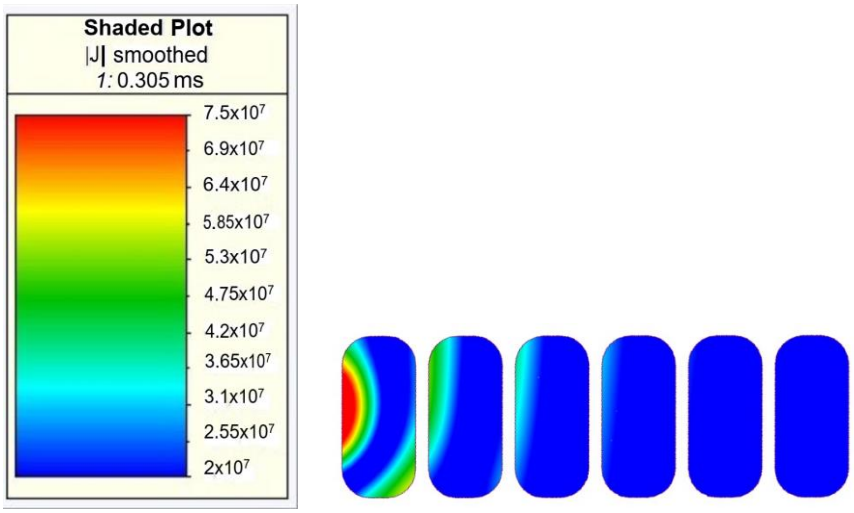

Figure 1. A general example showing the uneven current density distribution in hairpin conductors at high-frequency operations.

Several methods have been recently proposed to mitigate these phenomena in hairpin windings, especially the use of unconventionally shaped conductors near the slot opening [15,16]. However, all these studies assume the effect of the rotor field is negligible on skin and proximity effects, and thus the rotor usually is not modeled in the relevant analysis tools.

In addition, the positive effects of having reduced losses on the operating temperatures have been shown [16], as well as investigations on the cooling systems to be implemented when hairpin windings are adopted [17–20]. On the other hand, for a given hairpin layout, the effects of the operating temperature on the losses have not been investigated so far. In fact, while the result is known for the DC losses, i.e., the resistivity increases with temperature, the impact on AC losses is not obvious, especially for variable speed/frequency operations.

Therefore, although the importance of ohmic loss evaluation and thermal analysis for PMSMs equipped with hairpin windings has already been highlighted in previous studies,

the effect of temperature variation in hairpin conductors on AC losses at different working frequencies is not detailed.

Considering all the above, this work tries to fill these gaps by: (a) analyzing the effect of temperature on the overall losses, (b) investigating the impact of different permanent magnet rotor topologies on the overall losses, and (c) analyzing the effects on losses of both temperature and rotor topologies. The benchmark machine considered for the investigations at hand is a traction motor intended for racing car applications, whose full design process was proposed in [12], including a multi-objective optimization carried out aiming to maximize power density and minimize power losses. In this paper, first, the design of this benchmark motor is refined considering the realistic and commercial dimensions of hairpin conductors. Then, the focus is on the temperature and topology impact on DC and AC losses, which is the main aim of this research.

2. Background

In [12], a surface PMSM intended for a Formula SAE [21] application was designed. While its first version consisted of a random winding stator, in [12], a hairpin winding was chosen through a multi-optimization process, with excellent results being achieved in terms of torque density and efficiency. In Figure 2, the optimal machine obtained in [12] is reported, whereas Table 1 summarizes the main achievements compared to the random winding design.

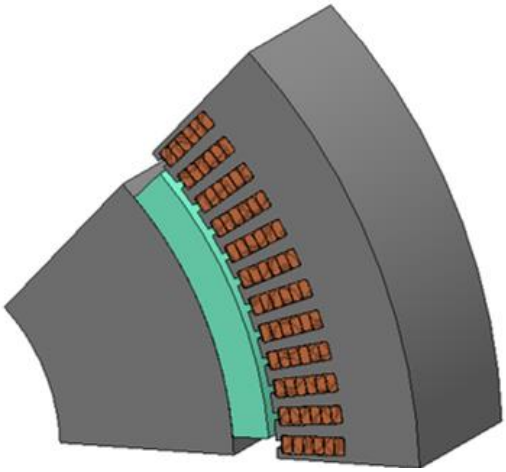

Figure 2. The geometry of the optimal motor from [12].

With the challenges related to losses and temperatures, the maximum frequency was kept below the 1 kHz range for this motor. In this study, an attempt was made to redesign the motor with a frequency range above 1 kHz using the same design process as in [12]. Furthermore, a thermal analysis was carried out to consider the real operating temperatures of the machine and their effect on the performance. The relevant aspects were indeed neglected in [12].

In [12], a special focus was given to the loss evaluation, especially in the copper, as one of the most critical factors to consider when designing an electrical machine with hairpin windings is the AC losses. The DC resistance, R_{DC}, of a machine phase depends on the total length of one coil, L_c, the number of turns in series N and parallel paths per phase, the cross-sectional area of the conductor, S_c, and the conductivity of the conductive material, σ_c. Considering a uniform current distribution, the losses associated with the DC resistance are the only contribution to the Joule losses. On the other hand, when skin and proximity effects occur, the AC losses must be carefully determined, and this is usually performed through the ratio between R_{AC} and R_{DC} [7]. In (1), k_R is the resistance factor, which is the ratio of the AC to DC resistance of the conductor, where z is the conductors' number in the slot and φ, ψ, and ξ are expressed as in (2), (3), and (4), respectively. The parameters h_{c0}

and b_c in (4) are the height and width of the conductors, respectively, while b is the slot width, ω is the supply frequency, and μ_0 is the permeability of the vacuum.

$$k_R = \frac{P_{AC}}{P_{DC}} = \varphi(\xi) + \frac{z^2 - 1}{3}\psi(\xi) \quad (1)$$

$$\varphi(\xi) = \xi \frac{\sinh 2\xi + \sin 2\xi}{\cosh 2\xi - \cos 2\xi} \quad (2)$$

$$\psi(\xi) = 2\xi \frac{\sinh \xi - \sin \xi}{\cosh \xi + \cos \xi} \quad (3)$$

$$\xi = h_{c0}\sqrt{\frac{1}{2}\omega\mu_0\sigma_c\frac{b_c}{b}} \quad (4)$$

Table 1. Comparison between the motor with random windings and the motor with hairpin windings [12].

Parameters	Round Winding	Hairpin Optimal Design
Mechanical power (KW)	40	40
DC link voltage (V)	600	600
Base speed (rpm)	12,740	12,740
Torque (Nm)	30	30
Surface current density (A/mm^2)	13	13
Linear current density (A/mm)	70	70
Peak current (A)	140	63.7
Fill factor	60%	85%
Pole number	6	8
slot/pole/phase	1	4
Axial length	65	26
Conductors/slot	11	6
Rotor radius	45	59
Tooth width	10	1.635
Yoke thickness	14	13.35
Outer radius	85	80.6
Power loss (kW)	2	1.42
Efficiency	95.2%	96.6%
Volume power density (MW/m^3)	16.75	74.4
Volume torque density (kNm/m^3)	13.21	55.76
Stator winding	Distributed, full-pitch, single layer	
Core material	M330-50A	
PM material	NdfeB-N28AH	

3. Practical Design

First Rotor Topology

In [12], an analytical model was used for optimization purposes, as it presents a reduced computation time as opposed to a finite element analysis (FEA). In this paper, the same analytical model was used, together with the multi-objective optimization, to further improve the surface PMSM. The same objectives were set, i.e., minimization of power loss and maximization of power density as in (5). The main difference between the design proposed in [12] and that presented in this paper is that practical considerations were carried out here, while these were previously neglected. First, the fill factor was updated from ≈85% to ≈65%, which is a more realistic value accounting for the conductors' corner radius, the insulation materials with their typical thicknesses, etc. Then, a higher operating frequency was considered, which was obtained by increasing the number of pole pairs from 4 to 5. After the implementation of the multi-objective evolutionary algorithm, whose results are reported in the Pareto front of Figure 3, a new optimal motor was achieved. This is shown in Figure 4 for the sake of completeness. A comparative summary between

the motor designed in [12] and the one carried out in the present contribution is shown in Table 2. Although the newly assumed fill factor was decreased, the power density and the overall losses (and thus the efficiency) remained basically the same as in the previous design. It is worth mentioning that all the comparative results reported in Table 2 were found without considering the end windings, as the estimations of their length, weight, losses, etc., were difficult to estimate analytically. However, the comparative exercise between the two motors is fully consistent.

The dimensions analytically obtained were used to build the machine geometry and a corresponding model within the FE-based software Simcenter MagNet.

$$P_{Density} = \frac{P_{out}}{Vol} \tag{5}$$

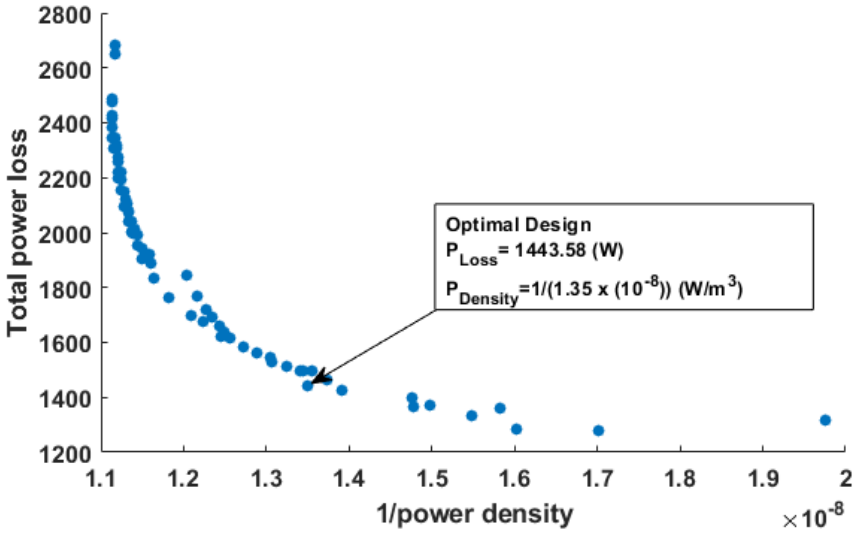

Figure 3. Optimization results for the design of the surface PMSM with hairpin winding.

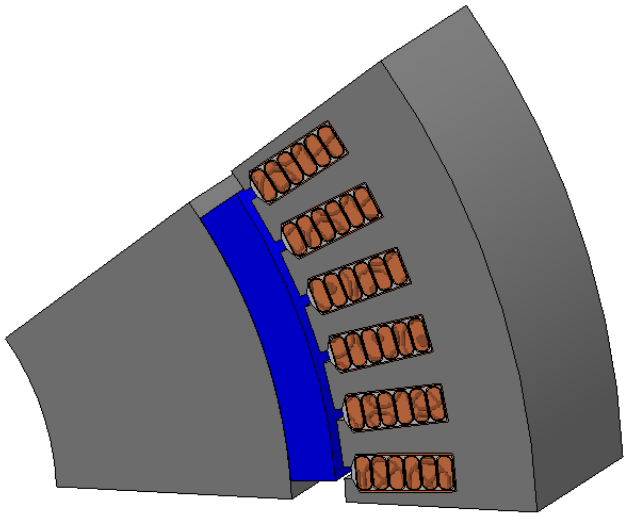

Figure 4. The geometry of the newly designed optimal motor.

Table 2. Design summary of the PMSM and comparison versus the previous design [12].

Parameter	New Optimal Motor	The Motor in [12]
Fill factor (%)	65	85
Outer stator diameter (mm)	173.27	161.2
Rotor diameter (mm)	124.8	118
Axial length (mm)	26	26
Slot− pole− phase	2	4
Pole number	10	8
Number of conductors per slot	6	6
Max. frequency (Hz)	1061.7	849.33
Efficiency (%)	96.1	96.6
Power density (MW/m^3)	74.1	74.5

4. Analysis of Ohmic Losses versus Temperature

As mentioned in the previous sections, one of the most critical challenges of hairpin windings is the high AC losses in the conductors, with that nearest to the slot opening being the most stressed (see Figure 1). This phenomenon is particularly evident at high operating frequencies. While the effect of frequency on AC losses is well-known and studied, the impact of the temperature has not been widely investigated, and thus this is the main target of this section.

First, considering the parameter k_R defined in (1), a value equal to 2 was taken as an acceptable index in terms of the amount of AC losses against DC ones. Considering this, the designed PMSM was analyzed via an FEA model, where the total DC and AC losses in the hairpin conductors were calculated at various frequency values, ranging from 0 Hz to ≈1.75 kHz. Figure 5 shows the DC and AC losses, where the frequency at which $k_R = 2$ is highlighted, i.e., ≈650 Hz. Furthermore, for the sake of completeness, PM losses and core losses were also evaluated which, added to the ohmic losses, contribute to the total power losses of the machine. These results are plotted in Figure 6. It is worth highlighting that these losses were found by considering an ambient temperature of 20 °C. However, all these loss contributions are temperature-dependent, especially the ohmic losses. In fact, the electrical resistivity of conductors changes linearly with temperature. It was therefore expected that, when the steady-state temperature was imposed on the conductors, the DC power loss would increase. On the other hand, the AC losses would not increase linearly as the AC resistance depends on the current distribution, and thus the overall losses at the steady-state temperature should be carefully investigated.

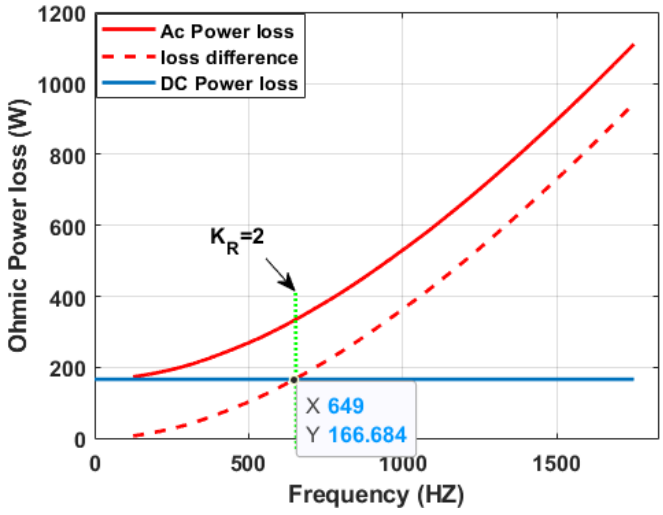

Figure 5. DC and AC losses versus frequency at ambient temperature (20 °C).

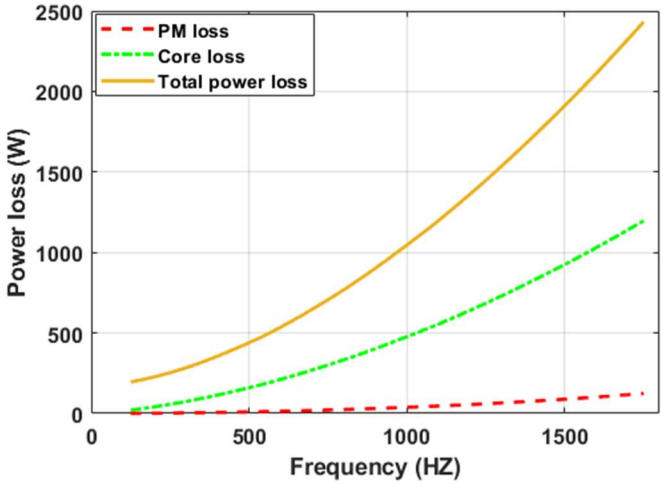

Figure 6. PMs, core, and total losses versus frequency at ambient temperature (20 °C).

Therefore, a thermal analysis was carried out considering the power losses found through the FEA (see Figures 4 and 5). The FE-based software Simcenter MagNet Thermal was used for such purposes. Nomex 430 was used as slot insulation, while Kapton was used as conductor insulation [22], and the slot was filled with Epoxy resin. Furthermore, as boundary conditions, the outer stator environment was covered by a water-jacket at a temperature of 50 °C, an additional convective heat transfer coefficient of 100 W/(m^2. °C) was assumed for the airgap, and a perfect insulator was considered for the shaft. Figure 7 illustrates the temperature map of the designed surface PMSM. It is worth highlighting that, although the PM temperature was ≈120 °C, no demagnetization challenges were expected as the selected PMs have the demagnetization knee in the third quadrant of the BH curve up to 150 °C.

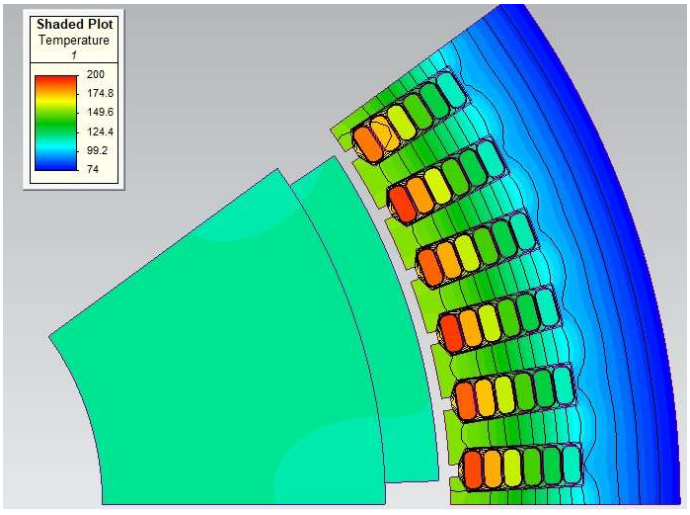

Figure 7. The FEA temperature map of the considered surface PMSM.

All the temperatures in the various parts of the machine were then recorded and transferred to the electromagnetic FEA model to calculate the losses at such temperatures, which are considered as the steady-state ones. As expected, the DC loss in the motor at steady state was higher than that at ambient temperature, as observed in Figure 8. Compared to the ambient case, the DC loss increased by ≈50%, but the slope of AC losses (red line) decreased by ≈45% when a linear approximation was performed around the point where k_R = 2. This resulted in an increase of the frequency value at which the AC-to-DC loss ratio, k_R, was equal to 2, i.e., it went from ≈650 (at ambient temperature) to ≈1200 Hz

(at steady-state temperature). The changes in the core and PM losses from ambient to steady state were not significant. Therefore, the total power loss significantly depends on ohmic losses. Figure 9 shows the total power losses in both conditions. It reports one of the most interesting results of this research. In fact, it informs that the total power losses at the thermal steady state were higher than those at ambient temperature up to ≈640 Hz, where the intersection between the two curves occurred (see the point 'M' in the figure). Above this intersection point, the total power losses at steady-state temperature become lower than those at ambient conditions. This finding leads to conclude that the operating temperature can play a very important role in the overall losses in hairpin windings, thus suggesting that a "temperature-oriented" motor design could enable higher efficiency levels in such types of electrical machines.

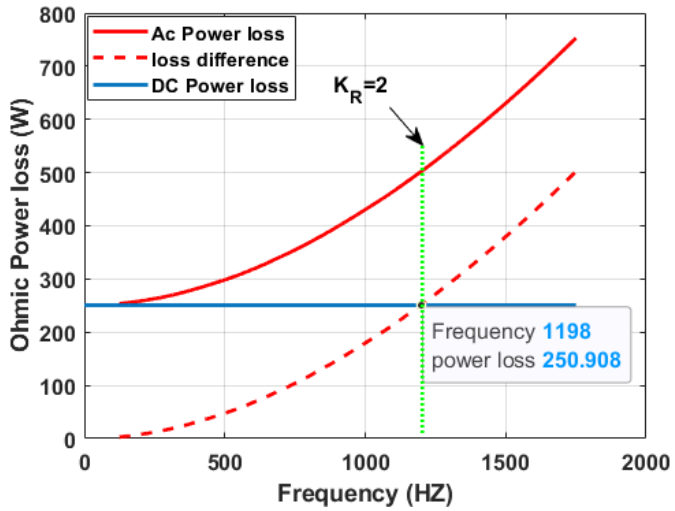

Figure 8. DC and AC losses versus frequency at the steady-state temperature.

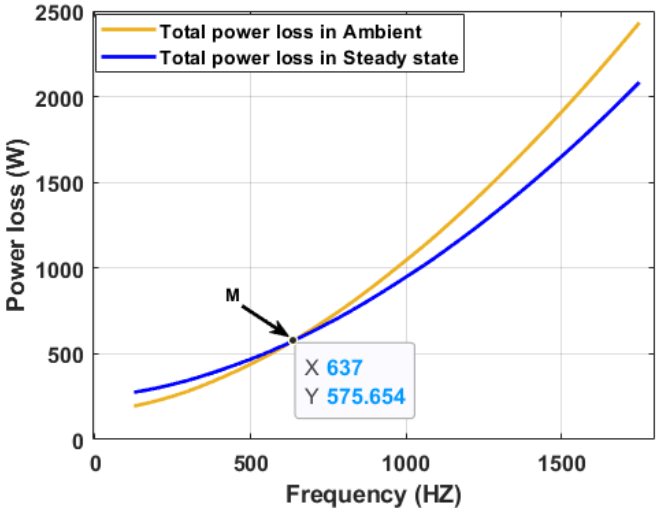

Figure 9. Comparison in terms of total losses versus frequency between ambient and steady-state temperature operation.

5. Analysis of Losses versus Rotor Topologies

5.1. Ohmic Losses versus Different Rotor Topologies

Besides the phenomena related to the temperature, another important aspect which is often overlooked when analyzing losses in hairpin windings is the effect of the rotor field. In this section, an analysis is carried out considering different rotor topologies while keeping the same stator as the designed PMSM. Figure 10 shows the four rotor

topologies investigated, where the PM volume was kept the same as the surface case. As seen, Topology 2 (Figure 9a) and Topology 3 (Figure 9b) were directly obtained from the surface layout (namely Topology 1) by embedding the magnets into the core. Figure 10c shows an interior PM rotor with the classical V shape (Topology 4), while Figure 10d shows an interior PM rotor with the classical Δ shape (Topology 5). It is worth mentioning that these topologies are not optimized as this would be out of the scope of this paper. The four considered topologies were investigated using the existing electromagnetic FEA model as per the surface PMSM. Figure 11 shows PM loss, total ohmic loss, and core loss versus frequency for the five rotor topologies. The temperature, initially, was set at the assumed ambient value of 20 °C. Topologies 4 and 5 featured lower overall losses, while Topology 2 was the one with higher losses, especially those in the core. This is true at any studied frequency value. It is also possible to observe that the motor frequency had no significant effect on PM losses in Topologies 3, 4, and 5. Concerning ohmic losses, Topologies 1 and 2 had no differences, while Topologies 3, 4, and 5 had a not-negligible effect, with the last one being the more efficient. In summary, focusing on the ohmic losses and taking as an example the losses at 800 Hz, the difference between Topology 1 and Topology 5 was 27.8%, thus proving that these aspects cannot be neglected in machines equipping hairpin windings. For the sake of completeness, the field maps at full-load conditions for all five topologies at 800 Hz are illustrated in Figure 11.

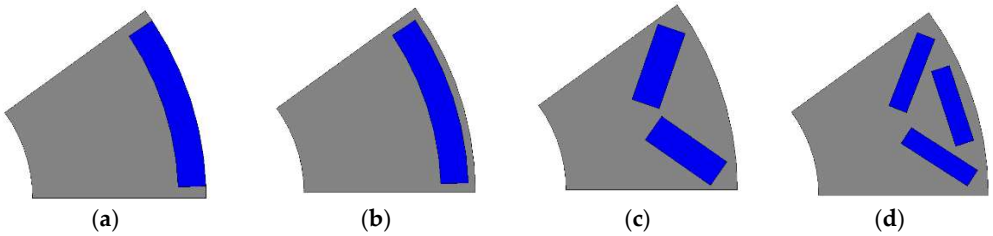

Figure 10. Rotor topologies: (**a**) Topology 2, (**b**) Topology 3, (**c**) Topology 4, and (**d**) Topology 5.

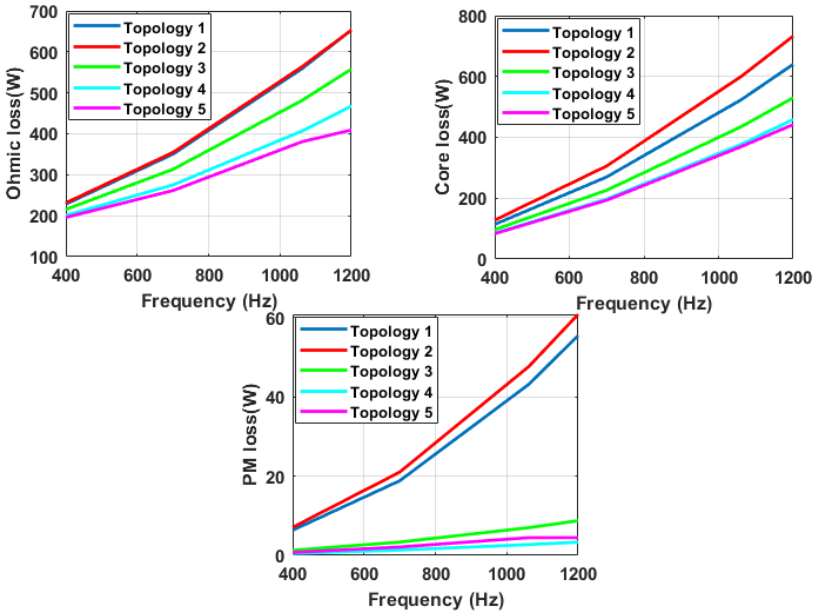

Figure 11. Comparison in terms of losses versus frequency among the five topologies considered.

5.2. Analysis of Ohmic Losses versus Both Temperature and Rotor Topologies

In this last section, the comparison among the rotor topologies is carried out considering the steady-state operating temperatures of the machines. To do so, the same procedure performed in Section 4 for Topology 1 was also carried out for the remaining

four topologies. This consisted of running a thermal analysis using the losses at 20 °C, obtaining an accurate temperature map, and recalculating the losses at these (steady state) temperatures. Figure 12 illustrates the DC power losses at ambient and steady-state temperature conditions for the five different rotor topologies. For Topology 1, the amount of DC loss was equal to that in Figures 5 and 8. The DC losses at ambient temperature were the same for all the topologies, as expected. On the other hand, a non-negligible difference was registered at steady-state temperature due to the different steady-state temperatures among the topologies. Figure 13 shows, for all five topologies, three frequency values: (1) the frequency at which $k_R = 2$ at ambient temperature, (2) the frequency at which $k_R = 2$ at steady-state temperature, and (3) the frequency intersection point where the total ohmic losses at steady-state temperature become lower than those at ambient temperature. It can be observed that this intersection point changed from one topology to another. In particular, the interior PM rotor layouts (Topologies 4 and 5) presented a higher-frequency intersection point, thus highlighting reduced room for improvement when a temperature-oriented design was adopted. For the sake of completeness, Figure 14 shows the current density maps for all five topologies at their corresponding frequency intersection points. Figure 15 reports the instantaneous current density in the conductors within one slot, considering the worst-case scenario. Topologies 4 and 5 present the higher values of current density for the conductors closest to the slot opening (first, second, and third conductors), whereas they feature lower current density values in the remaining ones.

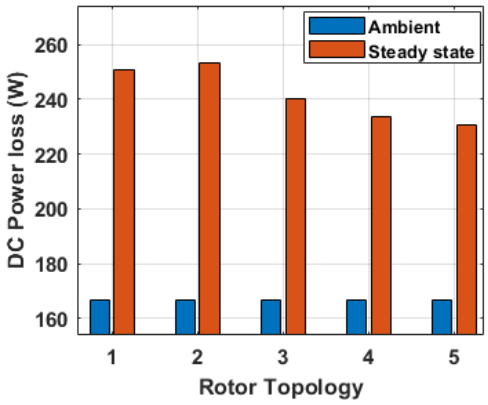

Figure 12. Comparison in terms of DC power losses among the five considered topologies, at both ambient and steady-state temperature conditions.

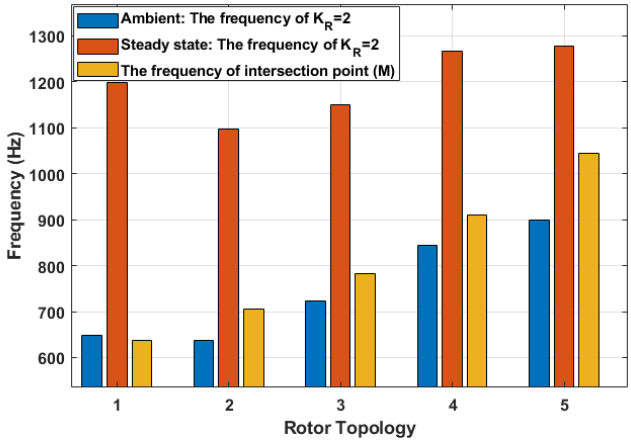

Figure 13. Comparison among the five considered topologies in terms of: (1) the frequency at which $k_R = 2$ at ambient temperature (in blue), (2) the frequency at which $k_R = 2$ at steady-state temperature (in red), and (3) the frequency intersection point where the total ohmic losses at steady-state temperature become lower than those at ambient temperature (in yellow).

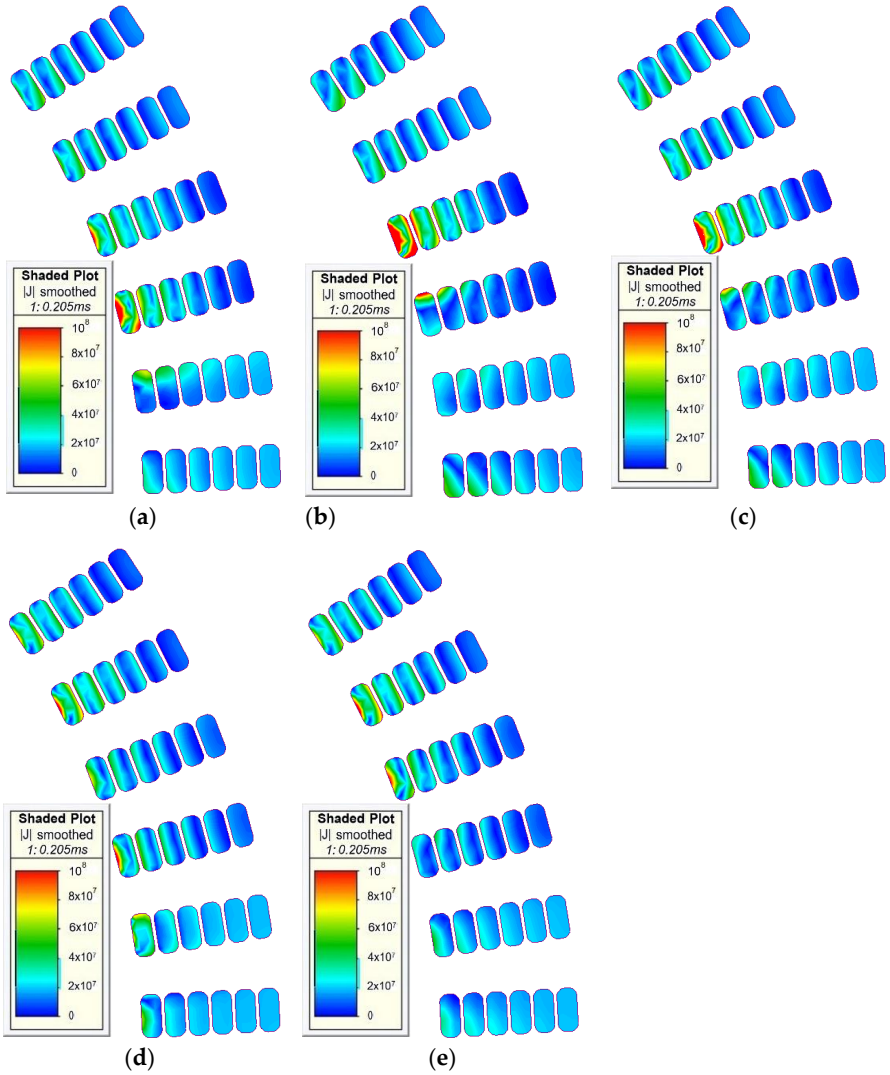

Figure 14. Instantaneous current density at the intersection frequency point in steady-state condition for the five rotor topologies, (**a**) First topology (SMPMSM), (**b**) Second topology, (**c**) Third topology (magnets embedded in the core), (**d**) fourth topology (the classical V shape), (**e**) fifth topology (the classical Δ shape).

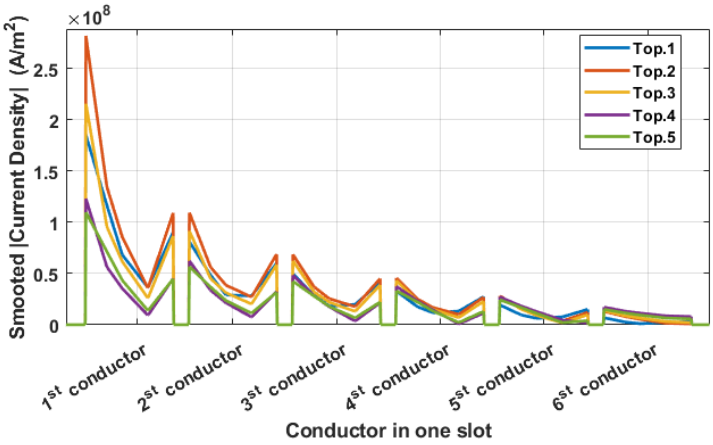

Figure 15. Instantaneous current density in the conductors within one slot of all five considered topologies, in the worst-case scenario.

6. Conclusions

In this paper, the focus was on ohmic losses in hairpin windings. The effects of both operating temperatures and rotor topologies were analyzed in detail, taking a surface-mounted PMSM intended for racing car applications as a case study.

The methodology consisted in:

(1) Evaluating the loss performance of the considered motor at an assumed ambient temperature of 20 °C via the electromagnetic FEA model.
(2) Evaluating the temperature map of the considered motor via the thermal FEA model considering the losses determined in (1).
(3) Evaluating the loss performance of the considered motor via the electromagnetic FEA model at the temperatures determined in (2).
(4) Repeating the above tasks for motors featuring different rotor topologies.

The main outcomes of this research are summarized in Figures 9 and 13, where it can be seen that there exists a frequency value at which the losses at higher temperatures than the ambient ones are lower. This is especially true for the benchmark case study, where this frequency value was equal to 637 Hz. A higher frequency value was found for the other four rotor topologies investigated, i.e., 704.7, 782.44, 909.25, and 1045.25 Hz, but still higher operating temperatures seem to be beneficial when AC losses are involved. The findings of this research indicated that a temperature-oriented design process for machines equipping hairpin conductors would be worthwhile in the context of reducing AC losses in this winding technology. Most of the findings reported in the paper are based on comparative analyses and, as such, they are fair and consistent. To have an experimental validation, it would be necessary to have a number of machines with different rotor topologies and test them at different temperatures and speeds. Our future research will attempt to overcome these challenges.

Author Contributions: Conceptualization, M.S and S.N.; methodology, M.S. and S.N.; software, M.S.; validation, M.S., S.N. and D.B.; formal analysis, M.S.; investigation, M.S.; resources, M.S.; data curation, M.S.; writing—original draft preparation, M.S.; writing—review and editing, S.N.; visualization, M.S.; supervision, S.N., D.B. and G.F.; project administration, D.B. and G.F.; funding acquisition, S.N., D.B. and G.F. All authors have read and agreed to the published version of the manuscript.

Funding: This research received no external funding.

Conflicts of Interest: The authors declare no conflict of interest.

References

1. Ranjbar, H.; Sharifzadeh, M. Electrification of Transportation. In *Industry 4.0 Vision for the Supply of Energy and Materials: Enabling Technologies and Emerging Applications*; Wiley: Hoboken, NJ, USA, 2022; pp. 269–296. [CrossRef]
2. Swaminathan, N.; Reddy, S.R.P.; Rajashekara, K.; Haran, K.S. Flying Cars and eVTOLs—Technology Advancements, Powertrain Architectures and Design. *IEEE Trans. Transp. Electrif.* **2022**, 1. [CrossRef]
3. Esmaeili, M.; Anvari-Moghaddam, A.; Muyeen, S.M.; Perić, V.S. On the Role of Renewable Energy Policies and Electric Vehicle Deployment Incentives for a Greener Sector Coupling. *IEEE Access* **2022**, *10*, 53873–53893. [CrossRef]
4. Kadavergu, A.; Anuradha, K.; Kumari, N.K. Development of Motor Gear Powertrain System for Electrical Vehicle. In *2021 Innovations in Power and Advanced Computing Technologies (i-PACT)*; IEEE: Manhattan, NY, USA, 2021; pp. 1–6. [CrossRef]
5. Pastura, M.; Nuzzo, S.; Immovilli, F.; Toscani, A.; Rumi, A.; Cavallini, A.; Franceschini, G.; Barater, D. Partial Discharges in Electrical Machines for the More Electric Aircraft—Part I: A Comprehensive Modeling Tool for the Characterization of Electric Drives Based on Fast Switching Semiconductors. *IEEE Access* **2021**, *9*, 27109–27121. [CrossRef]
6. Nuzzo, S.; Barater, D.; Gerada, C.; Vai, P. Hairpin Windings: An Opportunity for Next-Generation E-Motors in Transportation. *IEEE Ind. Electron. Mag.* **2021**, 2–10. [CrossRef]
7. Pyrhonen, J.; Jokinen, T.; Hrabovcova, V. *Design of Rotating Electrical Machines*; John Wiley & Sons: Hoboken, NJ, USA, 2013.
8. Rosskopf, A.; Brunner, C. Enhancing Litz Wire Power Loss Calculations by Combining a Sparse Strand Element Equivalent Circuit Method With a Voronoi-Based Geometry Model. *IEEE Trans. Power Electron.* **2022**, *37*, 11450–11456. [CrossRef]
9. Dimier, T.; Cossale, M.; Wellerdieck, T. Comparison of Stator Winding Technologies for High-Speed Motors in Electric Propulsion Systems. In Proceedings of the 2020 International Conference on Electrical Machines (ICEM), Gothenburg, Sweden, 23–26 August 2020; pp. 2406–2412. [CrossRef]

10. Popescu, M.; Goss, J.; Staton, D.A.; Hawkins, D.; Chong, Y.C.; Boglietti, A. Electrical Vehicles—Practical Solutions for Power Traction Motor Systems. *IEEE Trans. Ind. Appl.* **2018**, *54*, 2751–2762. [CrossRef]
11. Zhao, Y.; Li, D.; Pei, T.; Qu, R. Overview of the rectangular wire windings AC electrical machine. *CES Trans. Electr. Mach. Syst.* **2019**, *3*, 160–169. [CrossRef]
12. Soltani, M.; Nuzzo, S.; Barater, D.; Franceschini, G. A Multi-Objective Design Optimization for a Permanent Magnet Synchronous Machine with Hairpin Winding Intended for Transport Applications. *Electronics* **2021**, *10*, 3162. [CrossRef]
13. Soltani, M.; Nuzzo, S.; Barater, D.; Franceschini, G. Considerations on the Preliminary Sizing of Electrical Machines with Hairpin Windings. In Proceedings of the 2021 IEEE Workshop on Electrical Machines Design, Control and Diagnosis (WEMDCD), Modena, Italy, 8–9 April 2021; pp. 46–51.
14. Selema, A.; Ibrahim, M.N.; Sergeant, P. Mitigation of High-Frequency Eddy Current Losses in Hairpin Winding Machines. *Machines* **2022**, *10*, 328. [CrossRef]
15. Islam, M.S.; Husain, I.; Ahmed, A.; Sathyan, A. Asymmetric Bar Winding for High-Speed Traction Electric Machines. *IEEE Trans. Transp. Electrif.* **2020**, *6*, 3–15. [CrossRef]
16. Preci, E.; Nuzzo, S.; Valente, G.; Gerada, D.; Barater, D.; Degano, M.; Buticchi, G.; Gerada, C. Segmented Hairpin Topology for Reduced Losses at High-Frequency Operations. *IEEE Trans. Transp. Electrif.* **2022**, *8*, 688–698. [CrossRef]
17. Liu, C.; Xu, Z.; Gerada, D.; Li, J.; Gerada, C.; Chong, Y.C.; Popescu, M.; Goss, J.; Staton, D.; Zhang, H. Experimental Investigation on Oil Spray Cooling With Hairpin Windings. *IEEE Trans. Ind. Electron.* **2020**, *67*, 7343–7353. [CrossRef]
18. Reinap, A.; Andersson, M.; Márquez-Fernández, F.J.; Abrahamsson, P.; Alaküla, M. Performance Estimation of a Traction Machine with Direct Cooled Hairpin Winding. In Proceedings of the 2019 IEEE Transportation Electrification Conference and Expo (ITEC), Detroit, MI, USA, 19–21 June 2019; pp. 1–6. [CrossRef]
19. Zhang, F.; Gerada, D.; Xu, Z.; Liu, C.; Zhang, H.; Zou, T.; Chong, Y.C.; Gerada, C. A Thermal Modeling Approach and Experimental Validation for an Oil Spray-Cooled Hairpin Winding Machine. *IEEE Trans. Transp. Electrif.* **2021**, *7*, 2914–2926. [CrossRef]
20. Venturini, G.; Volpe, G.; Popescu, M. Slot Water Jacket Cooling System for Traction Electrical Machines with Hairpin Windings: Analysis and Comparison. In Proceedings of the 2021 IEEE International Electric Machines & Drives Conference (IEMDC), Hartford, CT, USA, 17–20 May 2021; pp. 1–6. [CrossRef]
21. Formula SAE Rules 2021 Version 1.0. Available online: www.fsaeonline.com/cdsweb/gen/DocumentResources.aspx (accessed on 1 July 2022).
22. Huang, X.; Jiang, B.; Alhallak, M.N.; Nategh, S.; Liu, Y.; Boglietti, A. Experimental Evaluation of Conductor Insulations Used in E-mobility Traction Motors. In Proceedings of the 2021 IEEE Workshop on Electrical Machines Design, Control and Diagnosis (WEMDCD), Modena, Italy, 8–9 April 2021; pp. 249–253. [CrossRef]